J Mater Sci (2020) 55:15275–15287

Materials for life sciences

Surface modification of a polylactic acid nanofiber membrane by zeolitic imidazolate framework-8 from secondary growth for drug delivery

Wenlong Liu[1], Hua Zhang[1,*], Wen Zhang[1,*], Mei Wang[1], Jiahui Li[1], Yun Zhang[1], and Hongyang Li[1]

[1] *State Key Laboratory of Separation Membranes and Membrane Processes, School of Materials Science and Engineering, Tiangong University, Tianjin, China*

Received: 12 May 2020
Accepted: 9 July 2020
Published online: 10 August 2020

ABSTRACT

Metal–organic frameworks (MOFs) materials have unique advantages such as high surface area and favorable structures in the drug delivery system. However, MOFs have the characteristics of easy aggregation and poor dispersion, which make the drug delivery not to reach the ideal effect. Developing biodegradable carrier for controlled drug delivery is still a challenging task. In this work, the zeolitic imidazolate framework-8/polylactic acid (ZIF-8/PLA) composite membranes were prepared by secondary growth method on the surface of electrospun nanofiber membrane. As the incubation time prolonged and the 2-methylimidazole (2-MIM) concentration increased, the size of ZIF-8 particles increased and the distribution of ZIF-8 became more uniform, resulting in increased the hydrophilicity and surface roughness. Furthermore, PLA/ZIF-8 nanofiber membranes had excellent pH response and drug release capacity. While only up to 40% of loaded drug was released in the buffer of pH value of 7.4, over 90% of drug was released at pH 5.5 due to the dissolution of ZIF-8 skeleton at acidic solution. It indicates that the pH-responsive PLA/ZIF-8 nanofiber membrane can be used as highly efficient drug carriers.

Address correspondence to E-mail: Hua1210@126.com; Zhangwen2050@hotmail.com

https://doi.org/10.1007/s10853-020-05066-8

GRAPHIC ABSTRACT

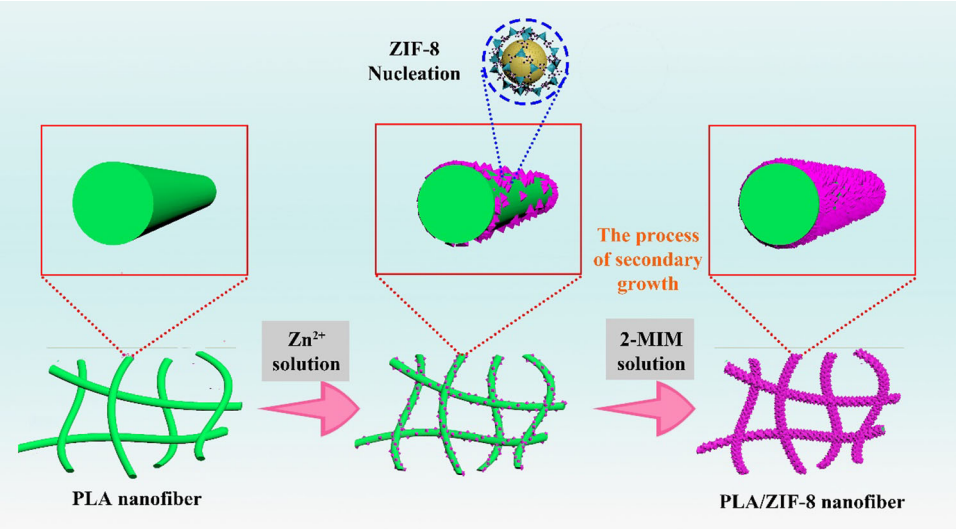

Introduction

With the change of people's lifestyle and the deterioration of the environment, cancer remains one of the greatest threats to human health [1]. Chemotherapy has become the first choice for cancer treatment because of its good systemic treatment effect, simple operation and good patient compliance. Therefore, the drug carriers required for chemotherapy need to be biocompatible. Drug delivery systems can be usually prepared with different types of drug carriers including nanoparticles, polymer–drug conjugates, solution-dispersed polymeric micelles or microspheres which can effectively control the release of drugs, to achieve the effect of treatment [2]. Hollow nanostructures have unique drug loading ability, which can lead to drug release through diffusion or degradation [3]. Recently, metal–organic frameworks (MOFs) of metals connected by organic linkers have been regarded as ideal drug nanocarriers [4–6]. MOFs are often used for gas separation [7], storage [8, 9], sensing [10], catalysis [11] and drug delivery [12, 13] due to its high surface area, tunable pore sizes, multifunctional properties and favorable structures [14]. Generally, two strategies, ex situ encapsulation where drug is put into contact with previously synthesized MOF and in situ encapsulation where drug is added to a MOF synthesis solution, have been used to achieve MOFs-based drug delivery [15]. The first method can cause drug leakage before the degradation of carriers and lead to low drug loading and uncontrolled drug release behavior. Another method in which the MOF structure is formed around the entrapped molecule realizes that the synthesis of MOFs and the drug loading are synchronized, avoiding drug leakage during the releasing process. However, the existence of strong interaction between drug and MOF has become an essential factor to influence drug loading. It is urgent to obtain an effective strategy to solve the low drug load and burst release behavior in MOFs carriers for drugs. ZIF-8 is regarded as one of the best MOFs for drug delivery because their skeleton can decompose in the acidic conditions.

ZIF-8 has a three-dimensional zeolite crystal structure formed by bridging zinc ions with the ligand of methylimidazolate. Compared with other ZIF structures, ZIF-8 has a small aperture (3.4 Å) and a large cavity size (11.6 Å) [16]. The ZIF-8 crystal consisted of the zinc ion source and imidazole salt linker has been well studied and established. In

traditional methods, soluble zinc salts, such as $Zn(NO_3)_2$, $ZnSO_4$ and $ZnCl_2$, can be used as a source of zinc ions [17]. As ZIF-8 has good chemical stability, thermal stability, degradability and biocompatibility, it is superior to other MOF in drug loading [18]. Since the dispersing properties of ZIF-8 particles are not sufficient to control drug release, a biocompatible matrix material is needed for ZIF-8 deposition.

Poly (lactic acid) (PLA), a kind of aliphatic polyester, is produced from renewable plant resources like corn and wheat [19]. Currently, PLA has received increasing attention in the field of biomedical materials because of its specific advantages of good biocompatibility, easy decomposability and degradation products are non-toxic to the human body. As a better sustained-release carrier, the membrane prepared with PLA has been proved to have good sustained-release and controlled-release effects [20, 21].

The electrospinning technique has attracted much attention for preparing three-dimensional nanoscale fiber membranes with large surface volume and high porosity [19]. The nanofiber membranes are ideal substrates for MOFs crystal deposition because of their specific structural parameters and chemical tenability [22]. The composites consisting of MOF and electrospinning nanofiber have been fabricated by a series of synthesis methods, including solvothermal method, secondary growth, interfacial synthesis, supramolecular assembly, and so on [23–26]. In particular, the secondary growth method has the advantage of relative low higher temperatures, simple process and easier control of the MOF growth size. Jinfu et al. reported the synthesis of the high-quality ZIF-8 membranes for gas separation on the commercial ceramic tubes with modification of an alumina layer via secondary growth method [27]. The quality and reproducibility of the ZIF-8 membrane were significantly improved by coating a PDMS layer, and the composite membrane showed high selectivity in the separation of C3H6/C3H8 mixture gases. Imran et al. prepared the polysulfone/ZIF-8 hollow fiber membranes using various loadings of ZIF-8 nanoparticles for natural gas purification [28]. The uniform dispersion of ZIF-8 particles across the membrane surface hindered CH_4 permeation with enhanced CO_2/CH_4 selectivity. Mingmin et al. noticed that the ZIF-8@cellulose nanofiber composite membranes fabricated by in situ growth of ZIF-8 on cellulose nanofibers exhibited a preferred CO_2 adsorption capacity and molecular-sieving mechanism played an important role in this composite membrane [29]. The high-performance porous composites consisting of MOF and nanofiber have attracted a great deal of attention and been applied in many fields, such as sensing, supercapacitors, catalysis and contaminant removal [30–33].

In this work, we prepared PLA/ZIF-8 nanofiber membranes by the secondary growth method. A layer of ZIF-8 nanoparticles was immobilized on the surface of the PLA nanofiber membranes. In addition, the effects of different experimental conditions on the growth of ZIF-8 were studied and the drug loading and releasing properties of the PLA/ZIF-8 nanofiber membranes were detected by tests.

Materials and methods

Materials

PLA (M_w = 16700) was purchased from Nature Works Co., Ltd. 2-methylimidazole ($C_4H_6N_2$, 2-MIM) and zinc nitrate hexahydrate ($Zn(NO_3)_2{\cdot}6H_2O$) were provided from Aladdin Reagent Co., Ltd. (Shanghai, China). Methanol (CH_3OH), *N*,*N*′-dimethylformamide (DMF) and dichloromethane (DCM) were purchased from Shandong Qilu Petrochemical Engineering Company Co., Ltd. (Shandong, China). Astragalus Polysacharin (APS) was purchased from Xi'an Feida Biotechnology Co., Ltd. (Shanxi, China). Disodium phosphate dodecahydrate (Na_2HPO_4) was obtained from Tianjin Guangfu Technology Development Co., Ltd. (Tianjin, China). Sodium chloride (NaCl), sodium hydroxide (NaOH) and potassium dihydrogen phosphate (KH_2PO_4) were purchased from Tianjin Sailboat Chemical Reagent Technology Co., Ltd. (Tianjin, China).

Experimental

Electrospinning

0.5 g PLA was dissolved in 10 mL of the mixture of DCM and DMF. 0.5 g 2-MIM and 0.2 g of PVP were added to the PLA solution with stirring for 25 min. The obtained solution was transferred into a plastic syringe for electrospinning at a feed rate of 1 $mL{\cdot}h^{-1}$. The nanofiber membranes were collected on an aluminum foil paper, the distance between the needle

and drum was 15 cm, and the used voltage was 20 kV.

Preparation of the PLA/ZIF-8 nanofiber membranes

Considering the strong influence of incubation time for the morphology, ZIF-8 particles grew on the surfaces of nanofiber membranes with various incubation time and various incubation concentrations of 2-MIM. As shown in Fig. 1, the PLA nanofiber membranes were soaked in 15 mL aqueous solution containing 1.5 mmol $Zn(NO_3)_2{\cdot}6H_2O$ for 1 h, which was conducive to attract more zinc ion form the small ZIF-8 as the growth core on the nanofiber surface. Then, nanofiber membranes were washed three times with water and added into 10 mL of 0.24 mol·L^{-1} 2-MIM aqueous solution at room temperature. The incubation time was 6 h, 12 h and 18 h, respectively. The other group nanofiber membranes were incubated in a 2-MIM solution with 10 mL concentration of 0.08 mol·L^{-1},0.16 mol·L^{-1} and 0.24 mol·L^{-1} at room temperature, respectively, for 18 h The nanofiber membrane was taken out, washed with methanol and air-dried at 50 °C

Characterization

The surface micromorphologies of the samples were observed using a field-emission scanning electron microscope (FESEM, Hitachi S-4800, Japan) at 10.0 kV acceleration voltage. Thermogravimetric (TG) analysis was carried out on a STA449F3 analyzer (Germany) from 30 °C to 800 °C under N_2 with a heating rate of 10 °C min^{-1}. The Fourier transform infrared (FT-IR) spectra of the membranes were obtained using a spectrometer (Bruker TERSOR37, Germany) at a resolution of 1 cm^{-1} in the range of 4000 cm^{-1}–500 cm^{-1}. XPS (Themo Fisher, *K*-alpha, China) was obtained by a Genesis 60 spectrometer equipped with an Al *Ka* radiation source (hv = 1486.4 eV). The roughness of the membrane surfaces was tested with a true color confocal microscope (Zeiss CSM700). The water contact angles (WCAs) were detected using a contact angle goniometer (JY-820, Chengde Texting Machine Co., Ltd.). The N_2 sorption analysis was conducted with an automated gas sorption analyzer (Autosorb-iQ-C) at 77 K applying the Brunauer–Emmett–Teller (BET) method for the specific surface area. The pore size distribution was obtained by using the HK models on the adsorption branch of the N_2 isotherm.

Drug release study

Drug loading capacity

PLA/ZIF-8 nanofiber membranes were immersed in the Astragalus Polysacharin (APS) solution with a concentration of 1 mg·mL^{-1} at room temperature for 12 h. The mixture was separated by centrifugation, and the supernatant was taken. The drug loading content (DL) of the supernatant was measured using a UV spectrophotometer and calculated via Eq. (1):

$$\mathrm{DL} = \frac{m_0 - m}{M} \times 100\% \quad (1)$$

where m_0 is the mass of APS in initial solution before loading, m is the mass of APS in the supernatant after centrifugation, and M is the mass of nanoparticles used [34, 35].

The effect of PLA/ZIF-8 nanofiber membranes on drug release in the simulated physiological environment was studied. PBS buffer solution with different pH (pH 7.4 and pH 5.5) was prepared. One gram of PLA/ZIF-8 nanofiber membranes loaded with the

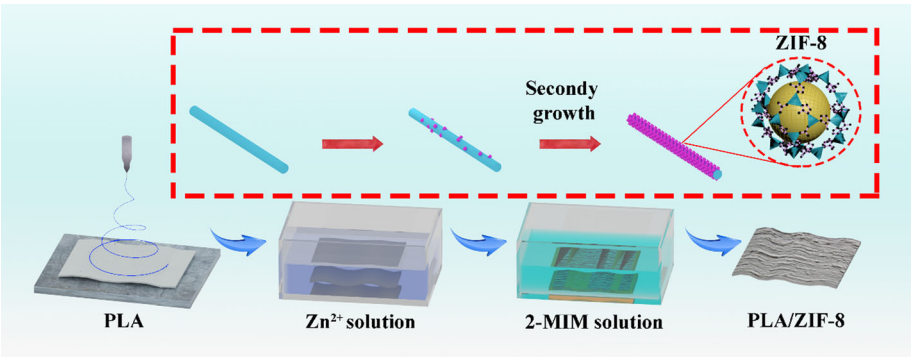

Figure 1 Schematic of the fabrication process of the PLA/ZIF-8 nanofiber membranes.

drug was put into a buffer solution, and the drug was released under the condition of constant temperature 37 °C with constant shaking. Then, the release status of the drug was indexed by measuring OD values at $\lambda = 600$ nm at regular intervals using a UV spectrophotometer. The release curve was drawn between the cumulative release percentage and time by the concentration corresponding to the OD value. PLA/ZIF-8 nanofiber membranes with different growth concentrations (0.04, 0.08, 0.12, 0.16, 0.20 and 0.24 mol·L^{-1}) were added to PBS solution with pH 5.5, and the OD value was measured at the same time interval.

Kinetics of drug release

Drug delivery characteristics were very important drug delivery systems in drug design. To analyze the mechanism of the process of sustained release, a kinetic model was usually used to describe the mechanism of sustained release [36]. For many drug delivery systems, the drug release process could usually be modeled using the classic Fick diffusion equation with appropriate boundary conditions or using a simplified Higuchi expression. Higuchi model described the release of a drug from an insoluble matrix as the square root of a time-dependent process based on the Fickian diffusion (Eq. 2) [37]:

$$Q_t = K_{HC} t^{1/2} \quad (2)$$

where Q_t is the amount of drug released in time t; K_{HC} is the release rate constant for the Higuchi model.

The Korsmeyer–Peppas model was one of the most ideal models for the analysis of drug sustained release in porous materials which could describe more comprehensively the kinetics of drug release from the matrices [38]. The Korsmeyer–Peppas model was expressed as:

$$\frac{M_t}{M_\infty} = K_{kp} t^n \quad (3)$$

where $\frac{M_t}{M_\infty}$ is the cumulative release of the drug at time t, K_{kp} is the kinetic constant, and n is the diffusion constant. The dynamic mechanism was determined by n, and when $n \leq 0.50$, the mechanism of drug release mechanism was consistent with the Fickian dispersion mechanism. When $0.50 < n < 1$, non-Fickian diffusion mechanism was observed. When $n \geq 1$, it was found to the skeleton corrosion mechanism.

Results and discussion

Characterization

The effect of the incubation time for the morphologies of PLA/ZIF-8 nanofiber membranes is shown in Fig. 2a–c in which the incubation time was 6 h, 12 h and 18 h, respectively. The uneven distribution of ZIF-8 particles on the nanofibers could be observed very clearly in Fig. 2a, and the amount of ZIF-8 particles increased with incubation time prolonged. The concentration of 2-MIM in the secondary growth condition of ZIF-8 particles significantly affected the morphologies of nanofiber membranes. The size of ZIF-8 increased with the improvement of the amount of the 2-MIM concentration in the condition of the same incubation time (18 h), which could be obtained from Fig. 2d–f. The entire nanofiber was covered with the ZIF-8 particles, when the incubation was 18 h and the concentration of 2-MIM was 0.24 mol/L. As shown in Fig. 2g, the presence of Zn and N elements indicates that the ZIF-8 particles had grown successfully in the surfaces of PLA nanofiber membranes.

FT-IR spectra of the PLA and PLA/ZIF-8 nanofiber membranes are shown in Fig. 3a. The spectrum of PLA/ZIF-8 nanofiber membranes showed all the characteristic bands of the functional groups of PLA with additional peaks at 1754 cm^{-1} and 1454 cm^{-1} which were assigned to the C=O stretching and the C–H bending vibration, respectively. The peaks at 1182 cm^{-1} and 1086 cm^{-1} were assigned to the symmetric and asymmetric mode of C–O–C stretching, respectively [39]. The presence of the new peaks at 3185 cm^{-1} and 2995 cm^{-1} in the spectra of the PLA/ZIF-8 nanofiber membranes, which arose from the aromatic and aliphatic C-H stretching of imidazole, together with the appearance of the amide group (1595 cm^{-1}), illustrated the successful incorporation of ZIF-8 into the nanofiber membranes [40, 41]. The chemical composition changes of PLA nanofiber membranes were confirmed by XPS analysis. As shown in Fig. 3c, $C1_s$ spectra of PLA nanofiber membranes were comprised of three major peaks at 288.78 eV, 286.68 eV and 284.58 eV, corresponding to the C=O group, C–O–C group and C–C

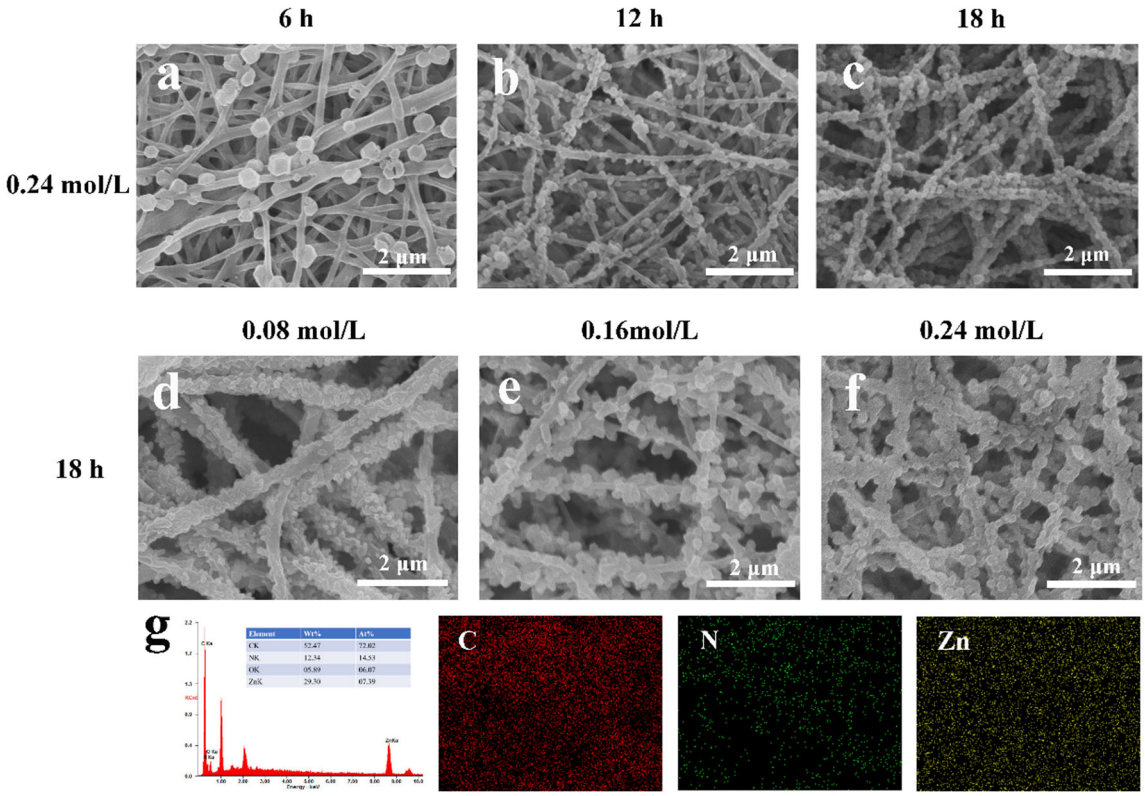

Figure 2 SEM images of PLA/ZIF-8 nanofiber membranes **a** 6 h, **b** 12 h, **c** 18 h, **d** 0.08 mol·L^{-1}, **e** 0.16 mol·L^{-1}, **f** 0.24 mol·L^{-1}. EDS images of **g** PLA/ZIF-8 nanofiber membranes.

bonds, respectively. It could be seen that elements N and Zn emerge in the XPS spectra of the PLA/ZIF-8 nanofiber membranes, which was consistent with EDS images. The high-resolution spectra and corresponding XPS data of N 1 s and Zn 2p peaks, shown in Fig. 3g and h, signified that the pyridinic N (398.68 eV), pyrrolic N (400.08 eV) and Zn–N bond (1044.28 eV and 1021.28 eV) were introduced onto the PLA/ZIF-8 nanofiber membranes, indicating that the ZIF-8 had been successfully coated onto the surface of nanofiber membrane surface [42, 43]. Another important observation was that the content of C–C bond in the PLA/ZIF-8 nanofiber membranes significantly increased. This phenomenon demonstrated that the amount of the organic ligand on the membrane surface ascends, which was in agreement with the morphology analysis.

Figure 4a shows the thermal gravimetric curves of PLA, PLA/ZIF-8 and PLA/ZIF-8-APS nanofiber membranes for a temperature range of 30–1000 °C in which the mass content of ZIF-8 in the nanofiber membranes had been tested. It was clear that the mass loss of PLA nanofiber membranes ranged from 150–450 °C and the residual mass at 800 °C was 4 wt% [44]. This temperature (150 °C) was almost the same as the melting point of PLA, which indicated that the TG measurement in this work was reliable. As for the PLA/ZIF-8 nanofiber membranes, there are two clearly separated mass loss stages in the range of 150 ~ 300 °C and 300–450 °C which were corresponding to pyrolysis of PLA nanofibers and degradation of ZIF-8 particles, respectively [45]. The residual mass of two samples of PLA/ZIF-8 nanofiber membranes was 38 wt% (12 h) and 40 wt% (18 h) when the ZIF-8 began to degrade, respectively. The highest content of ZIF-8 particles in the PLA/ZIF-8 nanofiber membranes (18 h) was almost 36%. It could be observed that the content of ZIF-8 particles in the nanofiber membranes increased slightly with the extension of incubation time corresponding to the result of SEM images, which further proved the success of ZIF-8 in situ growth on PLA nanofibers membranes. Compared with other samples, the TG curve of APS lost weight at 60 degrees due to the degradation of APS, indicating that APS was successfully loaded on the composite membrane.

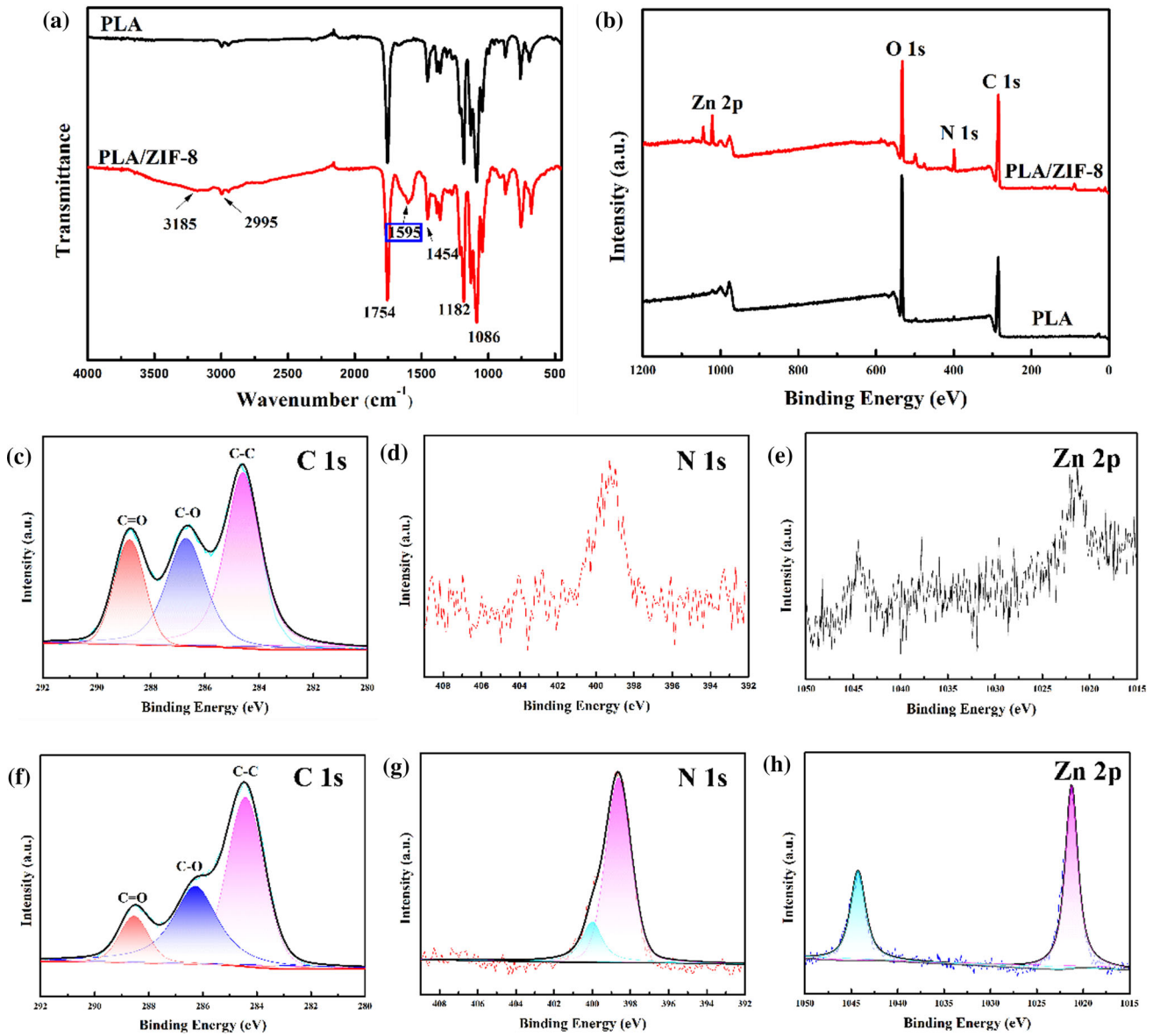

Figure 3 **a** FT-IR spectra and **b** XPS spectra of the PLA/ZIF-8 and PLA nanofiber membranes. XPS characterization of PLA nanofiber membrane illustrating **c** C 1s, **d** N 1s and **e** Zn 2p peak analysis. XPS characterization of PLA/ZIF-8 nanofiber membrane illustrating **f** C 1s, **g** N 1s and **h** Zn 2p peak analysis.

The crystallization property of pristine PLA nanofiber membranes was compared with that of the composite membrane, shown in Fig. 5b. The diffraction pattern for PLA nanofiber membranes showed one sharp peak 17.8° and two blunt peaks 24.6°, 25.8° which were associated with (200/110), (213) and (116) crystallographic planes which indicated PLA crystals were the typical orthorhombic crystal, respectively [46, 47]. As previously reported, the XRD spectra of ZIF-8 particles showed a typical ZIF-8 characteristic peaks (011), (002), (112) and (222) at around 7.3°, 10.4°, 12.8° and 18.1°, respectively [48, 49]. It was rather remarkable that there were three characteristic peaks of ZIF-8 particles (7.3°, 10.4° and 12.8°) in the spectrogram of the PLA/ZIF-8 nanofiber membranes indicating that all the diffraction peaks of PLA/ZIF-8 nanofiber membranes were well indexed, which revealed the successful growth of ZIF-8 on the surface of PLA nanofiber membranes. The porosity of PLA/ZIF-8 nanofiber membrane was further investigated by N_2 physisorption. The nitrogen-sorption isotherm of PLA/ZIF-8 nanofiber membranes

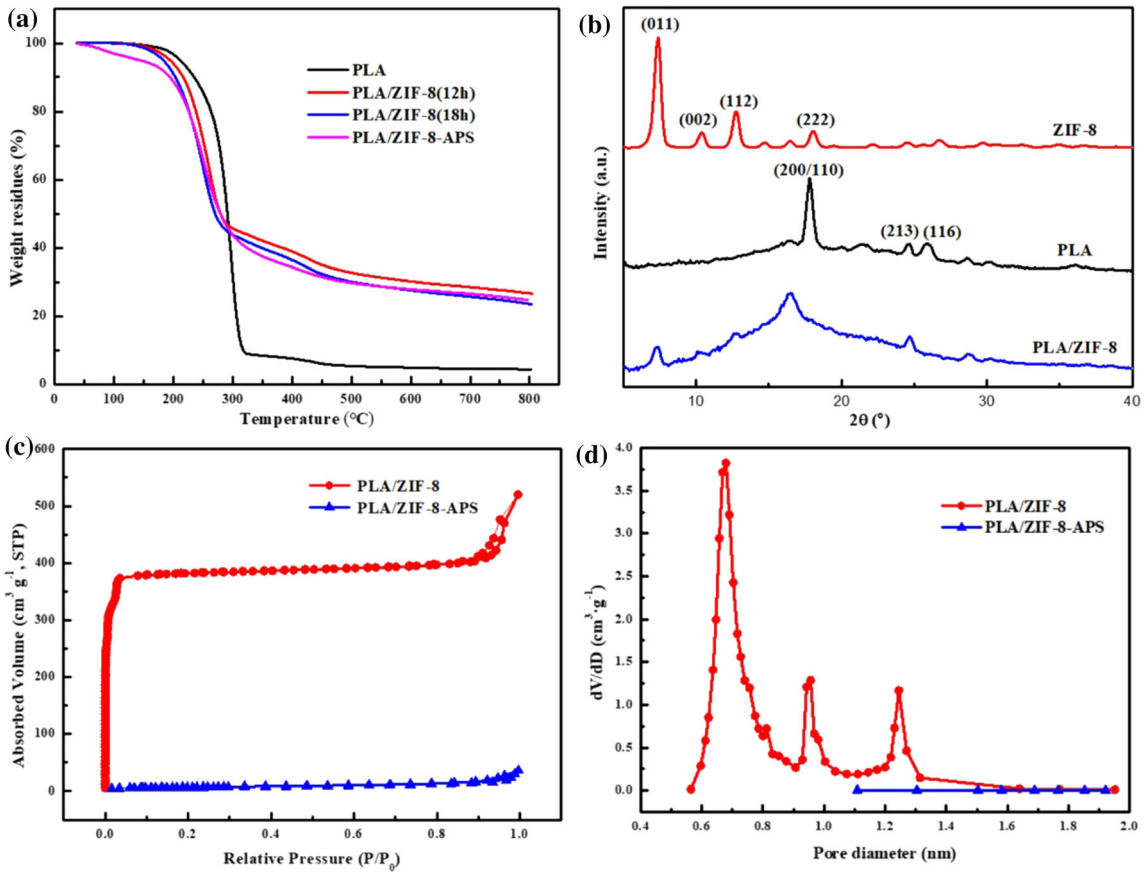

Figure 4 **a** TG curves of PLA, PLA/ZIF-8 (12 h), PLA/ZIF-8 (18 h) and PLA/ZIF-8-APS nanofiber membranes. **b** XRD pattern of ZIF-8, PLA and PLA/ZIF-8 nanofiber membranes. **c** Nitrogen adsorption–desorption isotherms and **d** the micropore size distribution curves of PLA/ZIF-8 and PLA/ZIF-8-APS nanofiber membranes.

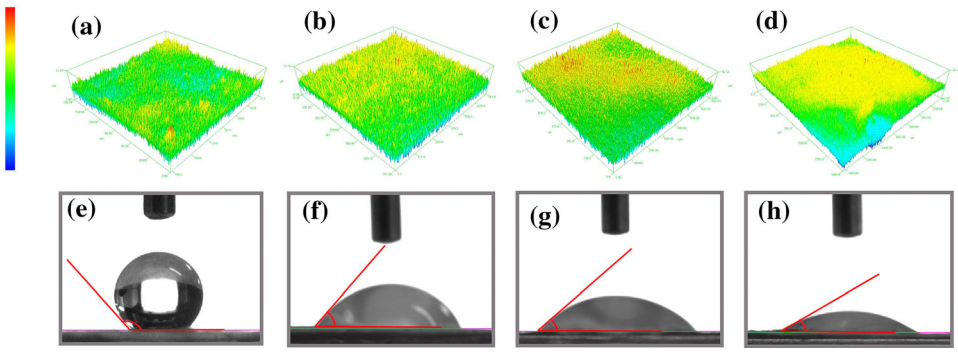

Figure 5 True color confocal microscope images and WCA of nanofiber membranes. **a** and **e** PLA, **b** and **f** PLA/ZIF-8 (6 h), **c** and **g** PLA/ZIF-8 (12 h), **d** and **h** PLA/ZIF-8 (18 h).

exhibited a type I with a sharp rise of nitrogen uptake at the low pressure, which was characteristic of microporous materials. The size distribution of microporous was evaluated by the HK models. Figure 4d shows that there were multiple peaks in the micropore size distribution curve of PLA/ZIF-8 nanofiber membranes, which can be attributed to the uneven growth of ZIF-8, and the average pore size was about 0.7 nm. The specific surface area of PLA/ZIF-8 nanofiber membranes decreased dramatically from 1174.7 to 32.5 $m^2 \cdot g^{-1}$ with the presence of APS, indicating that the PLA/ZIF-8 had excellent drug encapsulation performance.

Hydrophilicity and surface roughness

Surface roughness played an important role in the wettability of the membrane surface. According to

Table 1 Surface roughness and WCA of the nanofiber membrane

Sample	PLA	PLA/ZIF-8 (6 h)	PLA/ZIF-8 (12 h)	PLA/ZIF-8 (18 h)
Ra (um)	0.663	0.967	1.293	1.757
θ* (°)	129	52	47	31

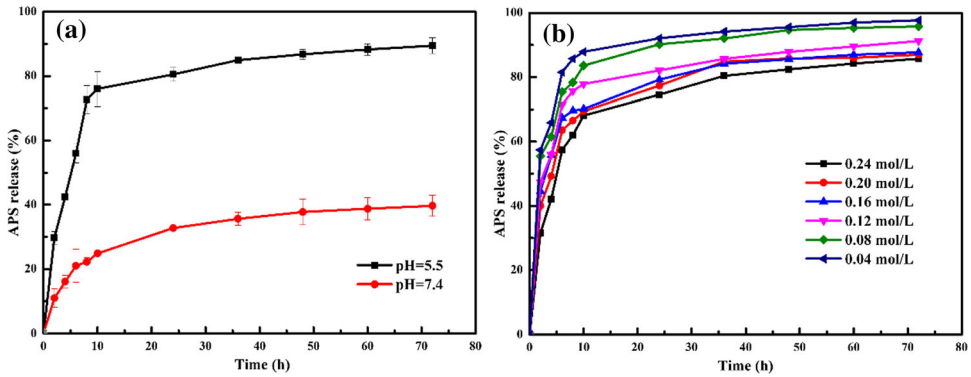

Figure 6 The effect of pH value **a** and the 2-MIM concentration **b** on release of APS.

Table 2 Zero-order, first-order, Higuchi and Korsmeyer–Peppas kinetics models of drug release from PLA/ZIF-8 nanofiber membranes

Sample	Zero-order kinetic		First-order kinetic		Higuchi model		Korsmeyer–Peppas model		
	K_0	R^2	K_1	R^2	K_{HC}	R^2	n	K_{kp}	R^2
pH 5.5	6.13	0.963	0.12	0.929	30.30	0.942	0.61	18.96	0.983
pH 7.4	1.69	0.928	0.09	0.862	8.60	0.985	0.48	7.90	0.981

the Wenzel equation, the wettability of the membrane surface will change with the change of surface roughness [50]:

$$\cos\theta^* = R_a \cos\theta \tag{4}$$

where θ^* and θ represent the WCA of the rough surface and flat surface, respectively, and R_a represents the roughness coefficient. The influence of preparation conditions on the surface roughness of PLA/ZIF-8 nanofiber membranes was studied, and the results are shown in Fig. 5 and Table 1. The nanofiber membranes changed from hydrophobicity to hydrophilicity, and the hydrophilicity became stronger with the content of ZIF-8 particles increasing on the nanofiber membranes. According to Fig. 5e and f, it was evident that the surface roughness of PLA/ZIF-8 nanofiber membranes was higher than that of the pure PLA nanofiber membranes. According to the Wenzel equation, for hydrophilic materials, the water contact angle would decrease with the increase in surface roughness [51–53]. With the prolonged incubation time of ZIF-8 particles, the roughness of nanofiber membranes got improved significantly as the description in the Wenzel equation that the R_a value would rise with the increase in the θ^* value. The main reason was that pure PLA nanofiber lacks hydrophilic groups and showed hydrophobicity. As the surface area of the nanofiber membranes with ZIF-8 particles increased, the contact area between ZIF-8 particles and water droplets increased due to hydrophilicity.

Drug release study

Figure 6 shows the cumulative release profiles of PLA/ZIF-8 nanofiber membranes. In neutral PBS, the cumulative release of APS was only about 40% even after 72 h at pH values of 7.4, in which APS was released in a very slow fashion from Fig. 6a. In contrast, it could be obviously seen that the system showed a faster drug release rate and more than 89% of the APS was released after 72 h at pH values of 5.5, exhibiting pH-responsive release capability. The high loading efficiency of the encapsulation of APS into PLA/ZIF-8 nanofiber membranes could reach up to 90% and the drug loading capacity could reach up to 460 mg·g^{-1}. These results implied that the loss of drug could be reduced during blood circulation (pH 7.4), while the drug release rate was suddenly accelerated after release into cancer cells. The drug release

rate was influenced by the content of ZIF-8 particles in the PLA/ZIF-8 nanofiber membranes. As shown in Fig. 6b, the drug cumulative release rate decreased with the concentration of 2-MIM increasing in the same conditions, which proved that the presence of ZIF-8 particles could effectively control drug release. Thus, the encapsulated drug might be effectively delivered to tumor tissues and cancer cells which should mitigate significant side effects.

The process of the drug cumulative release less than 80% was analyzed by mathematical models for studying the drug release mechanism of PLA/ZIF-8 nanofiber membranes. According to Figure S7 and Table 2, the drug release process at the pH value of 7.4 conformed to the Higuchi model in the four kinetic models mentioned above, which indicated that the APS release process was affected by diffusion. In addition, the n exponent was 0.48 at the pH value of 7.4 in the Korsmeyer–Peppas model further indicating that the release system was dominated by swelling diffusion [36]. It could be found from the Korsmeyer–Peppas model that n exponent was 0.61 at pH values of 5.5 indicating that the release kinetics process of the sustained-release system conformed to the anomalous (non-Fickian) diffusion mechanism which contained ZIF-8 skeleton dissolution and diffusion. In the acidic condition (pH 5.5), the ZIF-8 skeleton dissolution and drug diffusion processes occurred simultaneously, which was affected by the dissolution rate of the ZIF-8 skeleton. At the same time, the dissolution rate of the ZIF-8 skeleton was slow, which seriously blocked the drug diffusion process, achieving the purpose of controlling the drug release in the neutral conditions (pH 7.4).

Conclusion

In summary, a PLA/ZIF-8 nanofiber membrane was fabricated via secondary growth method and used for the drug delivery. The morphology of the PLA/ZIF-8 nanofiber membrane in the process of growth was significantly affected by the incubation time and ligand concentration, which can be observed by scanning electron microscopy. A uniform layer of ZIF-8 particles was covered on the surface of PLA nanofiber membrane after incubated for 18 h in the 2-MIM concentration of 0.24 $mol{\cdot}L^{-1}$. The hydrophilicity and roughness raised with the increase in ZIF-8 content on the surface of nanofiber membrane. The pH-responsive release of ZIF-8 was demonstrated by UV–Vis spectra. The kinetics fitting curve showed that the dissolution and diffusion of the ZIF-8 skeleton in an acidic solution resulted in a faster release of the composite membrane in a mild acidic buffer solution (pH 5.5). The prepared PLA/ZIF-8 nanofiber membrane shows promising prospects in the drug delivery.

Compliance with ethical standards

Conflict of interest The authors declare that there is no conflict of interest regarding the publication of this paper.

Electronic supplementary material: The online version of this article (https://doi.org/10.1007/s10853-020-05066-8) contains supplementary material, which is available to authorized users.

References

[1] Wang C, Xu L, Liang C, Xiang J, Peng R, Liu Z (2014) Immunological responses triggered by photothermal therapy with carbon nanotubes in combination with anti-CTLA-4 therapy to inhibit cancer metastasis. Adv Mater 26(48):8154–8162. https://doi.org/10.1002/adma.201402996

[2] Agrawal SK, Sanabria-DeLong N, Coburn JM, Tew GN, Bhatia SR (2006) Novel drug release profiles from micellar solutions of PLA-PEO-PLA triblock copolymers. J Control Release 112(1):64–71. https://doi.org/10.1016/j.jconrel.2005.12.024

[3] Moon GD, Choi SW, Cai X, Li W, Cho EC, Jeong U, Wang LV, Xia Y (2011) A new theranostic system based on gold nanocages and phase-change materials with unique features for photoacoustic imaging and controlled release. J Am Chem Soc 133(13):4762–4765. https://doi.org/10.1021/ja200894u

[4] Zhang HY, Li Q, Liu RL, Zhang XK, Li ZH, Luan YX (2018) A versatile prodrug strategy to in situ encapsulate drugs in mof nanocarriers: a case of cytarabine-IR820 prodrug encapsulated ZIF-8 toward chemo-photothermal therapy. Adv Func Mater 28(35):1802830. https://doi.org/10.1002/adfm.201802830

[5] Zheng H, Zhang Y, Liu L, Wan W, Guo P, Nystrom AM, Zou X (2016) One-pot synthesis of metal-organic frameworks with encapsulated target molecules and their applications for controlled drug delivery. J Am Chem Soc 138(3):962–968. https://doi.org/10.1021/jacs.5b11720

[6] Sun CY, Qin C, Wang XL, Yang GS, Shao KZ, Lan YQ, Su ZM, Huang P, Wang CG, Wang EB (2012) Zeolitic Imidazolate framework-8 as efficient pH-sensitive drug delivery vehicle. Dalton Trans 41(23):6906–6909. https://doi.org/10.1039/c2dt30357d

[7] Li W, Zhang G, Zhang C, Meng Q, Fan Z, Gao C (2014) Synthesis of trinity metal–organic framework membranes for CO_2 capture. Chem Commun 50(24):3214–3216. https://doi.org/10.1039/c3cc49815h

[8] Szczesniak B, Choma J, Jaroniec M (2018) Gas adsorption properties of hybrid graphene-MOF materials. J Colloid Interface Sci 514:801–813. https://doi.org/10.1016/j.jcis.2017.11.049

[9] Ishaq S, Tamime R, Bilad MR, Khan AL (2019) Mixed matrix membranes comprising of polysulfone and microporous Bio-MOF-1: Preparation and gas separation properties. Sep Purif Technol 210:442–451. https://doi.org/10.1016/j.seppur.2018.08.031

[10] Wang Y, Chen B, Zhang Y, Fu L, Zhu Y, Zhang L, Wu Y (2016) ZIF-8@MWCNT-derived carbon composite as electrode of high performance for supercapacitor. Electrochim Acta 213:260–269. https://doi.org/10.1016/j.electacta.2016.07.019

[11] Wang C, Wang H, Luo R, Liu C, Li J, Sun X, Shen J, Han W, Wang L (2017) Metal-organic framework one-dimensional fibers as efficient catalysts for activating peroxymonosulfate. Chem Eng J 330:262–271. https://doi.org/10.1016/j.cej.2017.07.156

[12] Zheng C, Wang Y, Phua SZF, Lim WQ, Zhao Y (2017) ZnO–DOX@ZIF-8 core-shell nanoparticles for pH-responsive drug delivery. ACS Biomater Sci Eng 3(10):2223–2229. https://doi.org/10.1021/acsbiomaterials.7b00435

[13] Yan L, Chen X, Wang Z, Zhang X, Zhu X, Zhou M, Chen W, Huang L, Roy VAL, Yu PKN, Zhu G, Zhang W (2017) Size controllable and surface tunable zeolitic imidazolate framework-8-poly(acrylic acid sodium salt) nanocomposites for pH responsive drug release and enhanced in vivo cancer treatment. ACS Appl Mater Interfaces 9(38):32990–33000. https://doi.org/10.1021/acsami.7b10064

[14] Zhao J, Li H, Li C, Zhang Q, Sun J, Wang X, Guo J, Xie L, Xie J, He B, Zhou Z, Lu C, Lu W, Zhu G, Yao Y (2018) MOF for template-directed growth of well-oriented nanowire hybrid arrays on carbon nanotube fibers for wearable electronics integrated with triboelectric nanogenerators. Nano Energy 45:420–431. https://doi.org/10.1016/j.nanoen.2018.01.021

[15] Liedana N, Galve A, Rubio C, Tellez C, Coronas J (2012) CAF@ZIF-8: one-step encapsulation of caffeine in MOF. ACS Appl Mater Interfaces 4(9):5016–5021. https://doi.org/10.1021/am301365h

[16] Ren G, Li Z, Yang W, Faheem M, Xing J, Zou X, Pan Q, Zhu G, Du Y (2019) ZnO@ZIF-8 core-shell microspheres for improved ethanol gas sensing. Sensors Actuators B: Chem 284:421–427. https://doi.org/10.1016/j.snb.2018.12.145

[17] Gong X, Wang Y, Kuang T (2017) ZIF-8-Based Membranes for Carbon Dioxide Capture and Separation. ACS Sustain Chem Eng 5(12):11204–11214. https://doi.org/10.1021/acssuschemeng.7b03613

[18] Chen X, Shi Z, Tong R, Ding S, Wang X, Wu J, Lei Q, Fang W (2018) Derivative of epigallocatechin-3-gallatea encapsulated in ZIF-8 with polyethylene glycol-folic acid modification for target and pH-responsive drug release in anticancer research. ACS Biomater Sci Eng 4(12):4183–4192. https://doi.org/10.1021/acsbiomaterials.8b00840

[19] Liu H, Wang S, Qi N (2012) Controllable structure, properties, and degradation of the electrospun PLGA/PLA-blended nanofibrous scaffolds. J Appl Polym Sci 125(S2):E468–E476. https://doi.org/10.1002/app.36757

[20] Bode C, Kranz H, Fivez A, Siepmann F, Siepmann J (2019) Often neglected: PLGA/PLA swelling orchestrates drug release: HME implants. J Control Release 306:97–107. https://doi.org/10.1016/j.jconrel.2019.05.039

[21] Shi X, Dai X, Cao Y, Li J, Huo C, Wang X (2017) Degradable Poly(lactic acid)/metal–organic framework nanocomposites exhibiting good mechanical, flame retardant, and dielectric properties for the fabrication of disposable electronics. Ind Eng Chem Res 56(14):3887–3894. https://doi.org/10.1021/acs.iecr.6b04204

[22] Liu C, Wu YN, Morlay C, Gu Y, Gebremariam B, Yuan X, Li F (2016) General deposition of metal-organic frameworks on highly adaptive organic-inorganic hybrid electrospun fibrous substrates. ACS Appl Mater Interfaces 8(4):2552–2561. https://doi.org/10.1021/acsami.5b10078

[23] Ostermann R, Cravillon J, Weidmann C, Wiebcke M, Smarsly BM (2011) Metal–organic framework nanofibers viaelectrospinning. Chem Commun 47(1):442–444. https://doi.org/10.1039/c0cc02271c

[24] Zhang Y, Zhang Y, Wang X, Yu J, Ding B (2018) Ultrahigh metal-organic framework loading and flexible nanofibrous membranes for efficient CO_2 capture with long-term, ultrastable recyclability. ACS Appl Mater Interfaces 10(40):34802–34810. https://doi.org/10.1021/acsami.8b14197

[25] Brown AJ, Johnson JR, Lydon ME, Koros WJ, Jones CW, Nair S (2012) Continuous polycrystalline zeolitic imidazolate framework-90 membranes on polymeric hollow fibers. Angew Chem Int Ed Engl 51(42):10615–10618. https://doi.org/10.1002/anie.201206640

[26] Brown AJ, Brunelli NA, Eum K, Rashidi F, Johnson JR, Koros WJ, Jones CW, Nair S (2014) Separation membranes. Interfacial microfluidic processing of metal-organic framework hollow fiber membranes. Science 345(6192):72–75. https://doi.org/10.1126/science.1251181

[27] Li J, Lian H, Wei K, Song E, Pan Y, Xing W (2020) Synthesis of tubular ZIF-8 membranes for propylene/propane separation under high-pressure. J Membr Sci. https://doi.org/10.1016/j.memsci.2019.117503

[28] Khan IU, Othman MHD, Jilani A, Ismail AF, Hashim H, Jaafar J, Zulhairun AK, Rahman MA, Rehman GU (2020) ZIF-8 based polysulfone hollow fiber membranes for natural gas purification. Polym Testing. https://doi.org/10.1016/j.polymertesting.2020.106415

[29] Jia M, Zhang X-F, Feng Y, Zhou Y, Yao J (2020) In-situ growing ZIF-8 on cellulose nanofibers to form gas separation membrane for CO_2 separation. J Membr Sci. https://doi.org/10.1016/j.memsci.2019.117579

[30] Li J, Yuan X, Wu Y-n, Ma X, Li F, Zhang B, Wang Y, Lei Z, Zhang Z (2018) From powder to cloth: facile fabrication of dense MOF-76(Tb) coating onto natural silk fiber for feasible detection of copper ions. Chem Eng J 350:637–644. https://doi.org/10.1016/j.cej.2018.05.144

[31] Wang L, Feng X, Ren L, Piao Q, Zhong J, Wang Y, Li H, Chen Y, Wang B (2015) Flexible solid-state supercapacitor based on a metal-organic framework interwoven by electrochemically-deposited PANI. J Am Chem Soc 137(15):4920–4923. https://doi.org/10.1021/jacs.5b01613

[32] Lee DT, Zhao J, Oldham CJ, Peterson GW, Parsons GN (2017) UiO-66-NH2 metal-organic framework (MOF) nucleation on TiO_2, ZnO, and Al_2O_3 atomic layer deposition-treated polymer fibers: role of metal oxide on mof growth and catalytic hydrolysis of chemical warfare agent simulants. ACS Appl Mater Interfaces 9(51):44847–44855. https://doi.org/10.1021/acsami.7b15397

[33] Efome JE, Rana D, Matsuura T, Lan CQ (2018) Metal–organic frameworks supported on nanofibers to remove heavy metals. J Mater Chem A 6(10):4550–4555. https://doi.org/10.1039/c7ta10428f

[34] Jiang P, Hu Y, Li G (2019) Biocompatible Au@Ag nanorod@ZIF-8 core-shell nanoparticles for surface-enhanced Raman scattering imaging and drug delivery. Talanta 200:212–217. https://doi.org/10.1016/j.talanta.2019.03.057

[35] Afshar S, Rashedi S, Nazockdast H, Ghazalian M (2019) Preparation and characterization of electrospun poly(lactic acid)-chitosan core-shell nanofibers with a new solvent system. Int J Biol Macromol 138:1130–1137. https://doi.org/10.1016/j.ijbiomac.2019.07.053

[36] Wang S (2009) Ordered mesoporous materials for drug delivery. Microporous Mesoporous Mater 117(1–2):1–9. https://doi.org/10.1016/j.micromeso.2008.07.002

[37] Siepmann J, Peppas NA (2011) Higuchi equation: derivation, applications, use and misuse. Int J Pharm 418(1):6–12. https://doi.org/10.1016/j.ijpharm.2011.03.051

[38] Korsmeyer RW, Gurny R, Doelker E, Buri P, Peppas NA (1983) Mechanisms of solute release from porous hydrophilic polymers. Int J Pharm 15(1):25–35. https://doi.org/10.1016/0378-5173(83)90064-9

[39] Dai X, Li X, Wang X (2018) Morphology controlled porous poly(lactic acid)/zeolitic imidazolate framework-8 fibrous membranes with superior PM2.5 capture capacity. Chem Eng J 338:82–91. https://doi.org/10.1016/j.cej.2018.01.025

[40] Qin YT, Peng H, He XW, Li WY, Zhang YK (2019) pH-responsive polymer-stabilized ZIF-8 nanocomposites for fluorescence and magnetic resonance dual-modal imaging-guided chemo-/photodynamic combinational cancer therapy. ACS Appl Mater Interfaces 11(37):34268–34281. https://doi.org/10.1021/acsami.9b12641

[41] Cai C, Zou Y, Xiang C, Chu H, Qiu S, Sui Q, Xu F, Sun L, Shah A (2018) Broccoli-like porous carbon nitride from ZIF-8 and melamine for high performance supercapacitors. Appl Surf Sci 440:47–54. https://doi.org/10.1016/j.apsusc.2017.12.242

[42] Wang D, Chen Y, Wang H, Zhao P, Liu W, Wang Y, Yang J (2018) N-doped porous carbon anchoring on carbon nanotubes derived from ZIF-8/polypyrrole nanotubes for superior supercapacitor electrodes. Appl Surf Sci 457:1018–1024. https://doi.org/10.1016/j.apsusc.2018.07.047

[43] Chang BD, Yang YQ, Jansen H, Ding F, Molhave K, Sun HY (2018) Confined growth of ZIF-8 Nanocrystals with tunable structural colors. Adv Mater Interfaces 5(9):1701270. https://doi.org/10.1002/admi.201701270

[44] Kang Y, Wang C, Shi X, Zhang G, Chen P, Wang J (2018) Crystallization, rheology behavior, and antibacterial application of graphene oxide- graft -poly (l -lactide)/poly (l -lactide) nanocomposites. Appl Surf Sci 451:315–324. https://doi.org/10.1016/j.apsusc.2018.04.271

[45] Zhang HF, Zhao M, Yang Y, Lin YS (2019) Hydrolysis and condensation of ZIF-8 in water. Microporous Mesoporous Mater 288:109568. https://doi.org/10.1016/j.micromeso.2019.109568

[46] Wang L, Gramlich WM, Gardner DJ (2017) Improving the impact strength of Poly(lactic acid) (PLA) in fused layer modeling (FLM). Polymer 114:242–248. https://doi.org/10.1016/j.polymer.2017.03.011

[47] Bhasney SM, Bhagabati P, Kumar A, Katiyar V (2019) Morphology and crystalline characteristics of polylactic acid

[PLA]/linear low density polyethylene [LLDPE]/microcrystalline cellulose [MCC] fiber composite. Compos Sci Technol 171:54–61. https://doi.org/10.1016/j.compscitech.2018.11.028

[48] Cravillon J, Nayuk R, Springer S, Feldhoff A, Huber K, Wiebcke M (2011) Controlling zeolitic imidazolate framework nano- and microcrystal formation: insight into crystal growth by time-resolved in situ static light scattering. Chem Mater 23(8):2130–2141. https://doi.org/10.1021/cm103571y

[49] Sun W, Zhai X, Zhao L (2016) Synthesis of ZIF-8 and ZIF-67 nanocrystals with well-controllable size distribution through reverse microemulsions. Chem Eng J 289:59–64. https://doi.org/10.1016/j.cej.2015.12.076

[50] Wong TS, Ho CM (2009) Dependence of macroscopic wetting on nanoscopic surface textures. Langmuir 25(22):12851–12854. https://doi.org/10.1021/la902430w

[51] Dorrer C, Ruhe J (2008) Drops on microstructured surfaces coated with hydrophilic polymers: Wenzel's model and beyond. Langmuir 24(5):1959–1964. https://doi.org/10.1021/la7029938

[52] Shardt N, Elliott JAW (2020) Gibbsian thermodynamics of wenzel wetting (was wenzel wrong? revisited). Langmuir 36(1):435–446. https://doi.org/10.1021/la7029938

[53] Bell MS, Borhan A (2020) A Volume-Corrected Wenzel Model. ACS Omega 5(15):8875–8884. https://doi.org/10.1021/acsomega.0c00495